Proceedings of ASME NHTC'01
35th National Heat Transfer Conference
Anaheim, California, June 10-12, 2001

NHTC2001-20002

HEAT TRANSFER ON A VEHICLE WINDSHIELD: AN EXPERIMENTAL AND NUMERICAL STUDY

Subrata Roy[1A], Karim Nasr[1B], Paresh Patel[1C] and Bashar AbdulNour[2]
[1]Mechanical Engineering Department
Kettering University, Flint, MI 48504, USA
[A]sroy@kettering.edu; [B]knasr@kettering.edu; [C]ppatel@kettering.edu

[2]Technology Development Department
Ford Motor Company, Dearborn, MI 48120
babdulno@ford.com

ABSTRACT:

Understanding the heat transfer interaction between an impinging jet and an inclined windshield surface is of paramount practical significance. In this paper, the heat transfer process is investigated utilizing a three-dimensional finite volume numerical method and renormalization group (RNG) theory based *k-e* turbulence model. The issuing incompressible jet is impinging upon the inside of an inclined windshield creating a thermal boundary layer and a fully three dimensional vortex structure. Numerical analyses using Fluent predict a detailed description of fluid flow patterns and heat transfer coefficients. Experimental investigations are performed on the inner surface for the purpose of obtaining local and average heat transfer coefficients and further validation of the numerical results.

INTRODUCTION:

The flow of an impinging air jet on an inclined surface addresses a number of practical applications. Industrial applications include defogging and deicing of a vehicle's windshield, Vertical/Short Take-off and Landing (V/STOL) engineering and film cooling of turbine blades. In this paper, the specific application of interest is air issuing from the defroster's nozzles of a vehicle and impinging on the glass windshield. Various factors can be examined for optimizing the flow performance for defrosting ice on the outside surface or clearing fog on the inside surface. The nozzle outlet must be capable of generating an airflow that disperses over the entire inner surface of the windshield. Extensive testing on vehicle systems and components would generally meet specific customer requirements. However, utilizing Computational Fluid Dynamics (CFD) tools, a designer can predict the performance of a system and optimize its objectives more cost-effectively by coupling the numerical results with experimental data.

The interaction of multiple cool air jets with a hot inclined wall generates complex flow fields that have been extensively investigated in the literature. Polat et al. (1989) presented a relatively recent review of numerical studies related to axisymmetric impinging jets. An experimental study for incompressible jets issuing into a cross flow was reported by Andreopoulos and Rodi (1984). More reviews were also documented by Martin (1977), Downs and James (1987) and Viskanta (1993).

A number of investigators have tackled the *specific* problem of air issuing from the defroster's nozzles and impinging on the inclined surface of a vehicle's windshield. The purpose of such investigations is to enhance the defroster's performance in providing clear areas free of frost or fog. Some have addressed the air flow distribution (AbdulNour and Foss, 1997), while others have utilized infrared (IR) thermal imaging (or thermography) for measurements of thermal patterns (Carignano and Pippione, 1990; Andreone et al., 1992). Willenborg et al. (1997) has documented defroster flow measurement details, where hot-wire velocity measurements in the defroster nozzle jet flow and in the immediate vicinity of the windshield interior surface were performed. Another experimental study (AbdulNour et al., 1997) was carried out to establish the parameters influencing the convection heat transfer coefficient *h* on the windshield. As a result, a two-dimensional wall jet for isothermal and uniform heat flux boundary conditions were determined experimentally using hot-wire, micro thermocouples, and thermal imaging surveys to quantify the velocity and temperature fields, respectively. The local value of h was found to be insensitive to the thermal boundary condition, especially in the turbulent downstream region. A recent survey of relevant investigations (Nasr and AbdulNour, 2000) points to the heat transfer coefficient being the primary controlling parameter influencing heat transfer between the fluid and the solid surface.

Although extensive experimental studies have been conducted on this application, reliable flow and thermal

measurements remain expensive and are limited by the amount of data that can be collected. Ikeda et al. (1992) presented the results of experimental and CFD analysis of airflow distribution on windows from defroster nozzles. Their CFD analysis employed an unstructured grid of a commercial code for the comparison of experimental and computational results. Sugano et al. (1994) developed a numerical method for predicting the defroster cleaning pattern using three-dimensional airflow analysis and showed a good agreement with experimental observations; stating that numerical analysis can be used effectively in predicting the defroster cleaning patterns before constructing prototypes.

In the present paper, the fluid-thermal characteristics of an impinging jet on a windshield are identified. Experimental measurements of local surface temperatures, using liquid crystals, and similar to the technique performed by Simonich and Moffat (1982), will be used to yield local heat transfer coefficients for an imposed heat flux. A map of heat transfer coefficients between the surface and the incoming jet is obtained. Corresponding three-dimensional numerical simulation is performed using a finite-volume algorithm for obtaining detailed temperature and flow distributions. The solution is validated with experimental data and the predicted local and average heat transfer coefficients on the internal surface of an inclined windshield are compared.

EXPERIMENTAL SETUP:

An experimental apparatus consisting of the HVAC module of a vehicle and a windshield was assembled. A thin heating pad, 0.3048 m wide and 0.4572 m long, was attached centrally to the outer surface of the windshield providing constant surface heat flux in that region. Air is forced onto the inclined windshield, via the blower of the HVAC module, impinges and hugs the large surface of the windshield, and disperses into the laboratory environment. A general schematic of the experimental apparatus is shown in Figure 1. The main base of the test stand is intentionally kept open for unrestricted placement, adjustment, and accessibility of the HVAC module components. To allow for the possible adjustment of the windshield's angle between the windshield and dashpad, two pillars, made of 3.81cm perforated angle, were affixed to the stand.

A representative windshield angle of a passenger vehicle was chosen as 39°, which is the angle used for the experiments. A pair of 12.7cm bolts was placed in the appropriate pillar holes to support the windshield at the desired angle. To power the blower of the HVAC module, a 12V AC-DC power converter was chosen, wired into the blower unit and tested. It should be noted that in the actual application, the air is heated via a heater core and impinges on the windshield. In the current experiment, unheated room-air impinges on a heated windshield. The windshield is heated partially on its outer surface via a thermal heating pad, as mentioned earlier. The heater is capable of producing approximately 540 watts. The back surface of the heating pad is insulated via a polystyrene insulation layer of a known R-value.

A variable resistor potentiometer was used in conjunction with two Digital Multi-Meters (DMM's), for the purpose of controlling the heat flux. One DMM was used to measure the voltage while the other yielded the current. Of course, the heating pad wattage (input) is the product of volts times amps. The convected heat by the flowing air is computed by: $Q_{conv} = Q_{input} - Q_{loss} - Q_{rad}$, where Q_{loss} is the rate of heat transfer, in watts, off the back surface of the heater. This heat loss was quantified based on the temperature of the back surface of the heater and the temperature of the outer surface of the insulation pad. Q_{rad} is the radiative heat transfer exchanged between the inner surface of the windshield and the surroundings, $Q_{rad} = esA(T_s^4 - T_{surr}^4)$.

NUMERICAL MODEL:

Figure 2 describes the schematic of a vehicle windshield and its associated air volume. The air jet, at temperature T_j, is issued at an angle ϕ through two rectangular openings and impinges upon the glass windshield of thickness *t*. The windshield is inclined at an angle α and has a heating pad that is centrally placed on the external surface of the windshield. The heating pad introduces a constant heat flux into the heated area. All necessary dimensions are given in the figure. The mean plug flow velocity in the injection pipe is *V*.

The system of equations for steady, turbulent, buoyancy-driven, incompressible jet flows, including the *k-e* model, has been studied in detail in the literature (Johari et al., 1999). For state variable $\mathbf{q} = [1 \quad u \quad v \quad w \quad k \quad e \quad T]^T$, the transformed equations for the intrinsic coordinate system x_i can be written as (Roy, 2000)

$$\frac{\partial \mathbf{f}^{x_i}}{\partial x_i} = \frac{\partial}{\partial x_i}\left(\mathbf{f}_u^{x_i} + \hat{\mathbf{f}}_u^{x_i}\right) + \mathbf{S} \qquad \text{.....(1)}$$

where **S** is the source term which includes Boussinesque approximation for the momentum equation, $\mathbf{f}^{x_i}$ is the convective flux vector, and $\mathbf{f}_u^{x_i}$ and $\hat{\mathbf{f}}_u^{x_i}$ are the diffusive flux vectors, given by:

$$\mathbf{f}^{x_i} \equiv rU^{x_i}\mathbf{q}, \quad \mathbf{f}_u^{x_i} = \tilde{A}_{eff}\, g^{x_i x_i} \frac{\partial \mathbf{q}}{\partial x_i},$$

$$\text{and } \hat{\mathbf{f}}_u^{x_i} = \tilde{A}_{eff}\, g^{x_i x_j} \frac{\partial \mathbf{q}}{\partial x_j}, i \neq j \qquad \text{.....(2)}$$

In the above equations U^{x_i} is the scaled ξ_i component of the contravariant velocity vector, and $g^{x_i x_j}$ are metric components introduced from the transformation of the equations from the physical (x_i: *x,y,z*) to the computational (x_i: *x,h,z*) space:

$$U^{x_i} = Ja\left(u_j \frac{\partial x_i}{\partial x_j}\right) \quad \text{and} \quad g^{x_i x_j} = Ja\left(\frac{\partial x_i}{\partial x_k}\frac{\partial x_j}{\partial x_k}\right) \text{.....(3)}$$

where *Ja* is the jacobian of the transformation matrix.

In this work, a renormalization group (RNG) based *k-e* model of Yakhot and Orszag (1986) is utilized. This model introduces two equations, one for the turbulent kinetic energy *k* and the other for its dissipation rate ε. These equations are included in the set of the transformed equations (1). The effect of this model is to introduce an additional viscosity, called turbulent viscosity, which is calculated as a function of density *r* by:

$$m_t = C_m r \frac{k^2}{e}$$

…….…....(4)

where C_m = 0.0845 (Lam, 1992). The turbulent viscosity is not a fluid property, but rather a property of the flow field. Its value is added to the molecular viscosity and yields an effective viscosity, μ_{eff}, which is used in the computational model. The *k* and *e* at the inlet are calculated from the following expressions:

$$k_{in} = \frac{3}{2}(T_u \cdot u)^2 \; e_{in} = \frac{k_{in}^{3/2}}{L_e} \text{ ……..…(5)}$$

where T_u is the turbulence level and L_e is a characteristic length of the domain.

Equations (1) and (2) constitute a system of non-linear algebraic equations. The system is linearized by relaxation. A streamline upwinding technique is employed for stabilizing numerical iterations. The pressure corrections are used to correct the pressure and the velocities. This predictor-corrector procedure constitutes one iteration. The solution is declared convergent when the maximum residual for each of the state variables becomes smaller than a convergence criterion of 10^{-4}.

RESULTS AND DISCUSSION:

Experimental Results:

The experiment was performed at a fixed blower setting and a heating pad power value of Q_{input} = 67.5 Watts. For this power input, the heat flux Q_{input}/A = 484.4 W/m^2. The heat flux loss through the insulation pad was calculated to be Q_{loss}/A = 29.43 W/m^2 and the net radiative flux off the inner surface of the windshield was computed to be Q_{rad}/A = 87 W/m^2. Therefore, the convective flux to the flowing air was found to be Q_{conv}/A = 368 W/m^2. Newton's law of cooling was employed to evaluate the local heat transfer coefficients:

$$h = \frac{Q_{conv}}{A(T_S - T_{in})} \text{ ……..…..(6)}$$

The incoming air temperature was recorded as T_{in} = 25.5°C by placing a type T thermocouple at the outlet of the blower ductwork i.e. at the defroster's nozzle exit plane. The local surface temperature of the windshield was measured by mapping the heated area of the windshield with strips of liquid crystals. These strips were placed on the inner surface of the windshield at various locations to provide a means to measure the temperature at specific locations. One hundred strips were used to capture an equivalent number of local temperatures. Each piece of liquid crystal has a temperature that it is sensitive to. When subjected to this temperature, it turns from black to another color. The color depends on how close to the designated temperature the strip is. For example, if the strip is exactly at the temperature, it turns green. When near the temperature but not at it, the strips turn blue or light red. Using these strips of liquid crystals, one hundred local surface temperature values were recorded across the heated area. A grid was formed on the windshield under the entire surface of the heating pad by drawing horizontal and vertical lines with a 2.54 cm spacing. This grid was used to record the location of the point at which the inner surface temperatures were detected. Embedded in the plastic are pieces of liquid crystal temperature sensing strips. As a result, a map of local surface temperatures was generated. Figure 3 displays an Excel-generated map (contours) of temperature values. A measured local surface temperature yields a local heat transfer coefficient via (6). Therefore, a map of local heat transfer coefficients can be generated as shown in Table 1. Note that each letter (A, B,..) in this table corresponds to a 2.54 cm dimension along the windshield, so that a grid is constructed of twelve cells laterally and eighteen cells longitudinally.

Errors in computing the value of the heat transfer coefficient could result from the measurement of the voltage, the current, the heat losses, the surface area, the surface temperature, and the incoming jet air temperature. Performing uncertainty analysis using the root-sum-square method (Moffat, 1998) and computing individual relative uncertainties yielded a 5.1% relative uncertainty in the value for the heat transfer coefficient. The average heat transfer coefficient over the heated area of the windshield was then computed as $\bar{h} = \frac{1}{A}\int h dA$ and found to be 29.4W/m^2 K. The numerical simulation, discussed in the next section, compares local temperatures as well as experimental and numerical heat transfer coefficients.

Numerical Predictions:

The schematic of the simulation volume was shown in Figure 2. A vertical (ϕ=0°) air jet at uniform temperature T_j = 25.5°C = 298.5K impinges upon the windshield of thickness *t* = 0.006m inclined an angle α = 39°. The injection ducts are rectangular slots with *n* = 0.241m and *h* = 0.019m. The distance between the slot centers *s* = 0.127m. The geometric dimensions of the windshield and its layout match exactly those set-up experimentally. In Figure 2, the bottom, side and top surfaces of the control volume and on the inside of the windshield, typical wall boundary conditions are used, i.e., the no-slip condition for the velocities and the wall functions for

the *k* and *e*. The axial velocity profile V is prescribed over the openings. The *k* and *e* are prescribed at the inlets by (5). Finally, a constant heat flux is applied through the heating pad. The downstream conditions are zero gradients for all state variables.

The average velocity at the inlet and the imposed heat flux values were determined experimentally and used for the numerical investigation. The mean flow velocities in the injection pipe is specified as V = 8m/sec. The heating pad for the numerical simulation is bounded by l = 0.457m in the longitudinal direction and w = 0.305m in the lateral direction. A uniform heat flux of 368 W/m² is applied on this area of the windshield. The inlet section is located at r = 0.134m and the exit at D = 0.896m. The other dimensions as shown in Figure 2 are: L = 1.447m, H = 0.719m, u = 0.569m, and m = 0.131m. Despite the symmetry of the geometric configuration, the entire domain is considered for analysis. The material properties of air and windshield glass are shown in Table 2.

A computational mesh of 127,156 tetrahedral finite volumes was created using commercial Hypermesh software (2000). The maximum distance between the wall and the first grid point varies between y^+ of 2.5 for the windshield to y^+ of 15 for the coarsest mesh. The turbulence level in (5) was chosen equal to 10% (*i.e.*, T_u=0.1) following the study in Chernobrovkin and Lakshminarayana (1999). It should be noted that factors such as mesh density, cell geometry, turbulence model, degree of approximation of the describing equations, error criterion for convergence, and numerical control parameters, can impact the speed and accuracy of the numerical solution.

The three-dimensional Navier-Stokes equations (1)-(2) are solved for this fluid-thermal system using a finite volume commercial code, Fluent (1998). The CFD solutions are documented in Figures 4 through 8. Figure 4 is a three-dimensional view of the air-flow characteristics inside the computational domain showing outlines of the inclined windshield, the heating pad, the inlets (defroster's nozzles), and the side walls. Tracking twelve particles released from each inlet shows complex three-dimensional pathlines of fluid flow.

Velocity vectors plotted on two-dimensional cross-section of the simulation volume at x = 0.144m captures the vortical flow patterns in Figure 5, exhibiting recirculation and flow issuing regions. The impinging fluid forms a bound vortex structure on this plane between the jets bending the fluid downward. The jets coming out of the defroster openings appear to the flow deflected by the windshield as "solid". A sharp velocity and temperature gradient is formed upstream of the jet while a "wake" region develops downstream of the jet. In the latter, a pair of bound vortices per jet is formed, which bends the jet both downward and upward, producing the well-known kidney shape in speed line contours.

Flow deflected off the inclined surface and spreading throughout the simulation volume may form vortices of different size. Figure 6 illustrates the temperature variation caused by the vortical structures on a selected vertical *yz*-plane at x = 0.52m. The jet impingement process tremendously affects the temperature distribution on the windshield. The air attached to the windshield is coming off the plane at the top of the plot. This complex three-dimensional nature of the fluid flow has significant influence on the heat transfer process between the jet and the inclined surface as well as inside the simulation volume. Higher velocity near the wall causes a local cooling effect due to higher convective heat transfer. The temperature contours on the inside surface of the windshield under the heated area in Figure 7, shows an overall comparison between the experimental data (Figure 3) and CFD prediction of thermal patterns. Note that the regions where the jets impinge upon the wall are about 7 (yellow) to 10 (green) degrees cooler than the top section (red) of the heating pad where much less heat is convected out.

The predicted temperature distribution on the inside of the heating pad should also be compared with the experimental data on a point-by-point basis. A detailed comparison of predicted and experimental temperature distribution done on seventeen points on two *z*- locations on the inside of the windshield is shown in Figure 8. The documented result validates the numerical prediction within 1-3°C of the measured temperature values. Corresponding heat transfer coefficients h, computed via (6), are also plotted in the same figure. The corresponding average heat transfer coefficient from the predicted numerical results was found to be $\bar{h} = 25.68\ \mathrm{W/m^2 K}$.

CONCLUSIONS:

This paper addressed numerical and experimental studies of air jets impinging on an inclined surface. Experimental measurements of surface temperatures, using liquid crystals, yielded a map of local heat transfer coefficients between the surface and the incoming jet for an imposed heat flux. Corresponding three-dimensional numerical simulation was performed using a finite-volume algorithm for obtaining detailed temperature and flow distributions. The numerical simulation correlated reasonably well with the experimental results and further explained the flow characteristics and thermal patterns. A detailed comparison on 34 locations under the heating pad validated the numerical predictions within 1-3°C of the measured temperature values. It has thus been established that numerical simulation could be used to analyze practical problems with varying degrees of difficulty. Further investigation should aim at the experimental quantification and correlation of the local convection heat transfer coefficient in the flow impingement region.

REFERENCES:

AbdulNour, B. S., and Foss, J. F., 1997, "Computational and Experimental Predictions of Automotive Windshield Flow", Proceedings of ASME Fluids Engineering Division Summer Meeting; ASME Paper No. FEDSM97-3022.

AbdulNour, R. S., Willenborg, K., Foss, J. F., McGrath, J. J., and AbdulNour, B. S., 1997, "Measurements of the Convective Heat Transfer Coefficient for a Two-Dimensional Wall Jet: Uniform Temperature and Uniform Heat Flux Boundary Conditions",

Proceedings of ASME Heat Transfer Division, M.E. Ulucakli et al., Ed., HTD-Vol. 3, pp. 109-116.

Andreone, L., Burzio, G., Damiani, S., and Romitelli, G., 1992, "Automatic Measurement of Defrosting/Defogging Process", 2nd Int. Conf. on Vehicle Comfort Ergonomic, Vibrational, Noise, and Thermal Aspects, ATA Paper 92A272.

Andreopoulos, J. and W. Rodi, 1984, "Experimental Investigation of Jets in a Crossflow", *Journal of Fluid. Mechanics*, vol. 138, pp. 93-127.

Carignano, M. and Pippione, E., 1990, "Optimization of Wind-Screen Defrosting for Industrial Vehicles Via Computer Assisted Thermographic Analysis", FIJITA Paper 905237.

Chernobrovkin, A., and B. Lakshminarayana, 1999, "Turbulence Modeling and Computation of Viscous Transitional Flows for Low Pressure Turbines", *Journal of Fluids Engineering*, vol. 121, pp. 824-833.

Downs, S. J. and James, E. H., 1987, "Jet Impingement Heat Transfer—a Literature Survey", ASME Paper No. 87-HT-35.

FLUENT© 5 User's Guide, Fluent Inc., 1998, Volume 1-4, Lebanon, NH.

Hyperworks© 4.0 Online Users Manual, Altair Engineering, 2000, Troy, MI.

Ikeda, Y., Katoh, N., Ishii, N., and Kuriyama, T., 1992, "Numerical Analysis of the Airflow on Windows from Defroster Nozzles" (in Japanese), JSAE Paper 924076.

Johari, H., M. Pacheco-Tougas and J.C. Hermanson, 1999, "Penetration and Mixing of Fully Modulated Turbulent Jets in Crossflow", *AIAA Journal*, vol. 37, pp. 842-850.

Lam S. H., 1992, "On the RNG Theory of Turbulence," Physics of Fluids A, Vol. 4, pp. 1007-1017.

Martin, H.,1977, "Heat And Mass Transfer Between Impinging Gas Jets And Solid Surfaces". In Advances in Heat Transfer, Academic Press, New York, Vol. 13. pp. 1-60.

Moffat, R. J., 1988, "Describing the Uncertainties in Experimental Results," Experimental Thermal and Fluid Science, Vol. 1, pp. 3-17.

Nasr, K.J. and AbdulNour. B.S. (2000) 'Defrosting of Automotive Windshields: Progress and Challenges', Int. J. of Vehicle Design. Vol. 23. Nos. ¾, pp. 360375.

Polat, S., Huang, B., Mujumdar, A.S., and Douglas, W.J.M., 1989, "Numerical Flow and Heat Transfer Under Impinging Jets: A Review," Annual Review of Numerical Fluid Mechanics and Heat Transfer, Vol.2 pp.157-197.

Roy, S., 2000, "Numerical Investigation of the Blade Cooling Effect Generated by Multiple Jets Issuing at an Angle into an Incompressible Horizontal Cross Flow," Numerical Heat Transfer – Part A, Vol. 38, no. 7, pp. 701-718.

Simonich, J. C. and Moffat, R.J., 1982, "New Technique for Mapping Heat Transfer Coefficient Contours," Rev. Sci. Instrum., 53(5), 678-683

Sugano, M., Yamada, T., Takesue, Y., and Yasuki, T., 1994, "Numerical Analysis of Defroster Cleaning Pattern" (in Japanese), JSAE Paper 9432912.

Viskanta, R., 1993, "Heat Transfer to Impinging Isothermal Gas and Flame Jets". *Experimental Thermal and Fluid Science*, 6, 111-134

Willenborg, K., Foss, J. F., AbdulNour, R. S., McGrath, J. J., and AbdulNour, B. S., 1997, "A Model Defroster Flow", Proceedings of the Eleventh Symposium on Turbulent Shear Flows, Vol. 2, pp. 15.25-15.30.

Yakhot, V. and Orszag, S.A., 1986, "Renormalization Group Analysis Of Turbulence. I. Basic Theory," Journal of Scientific Computing, Vol. 1, pp. 3-51.

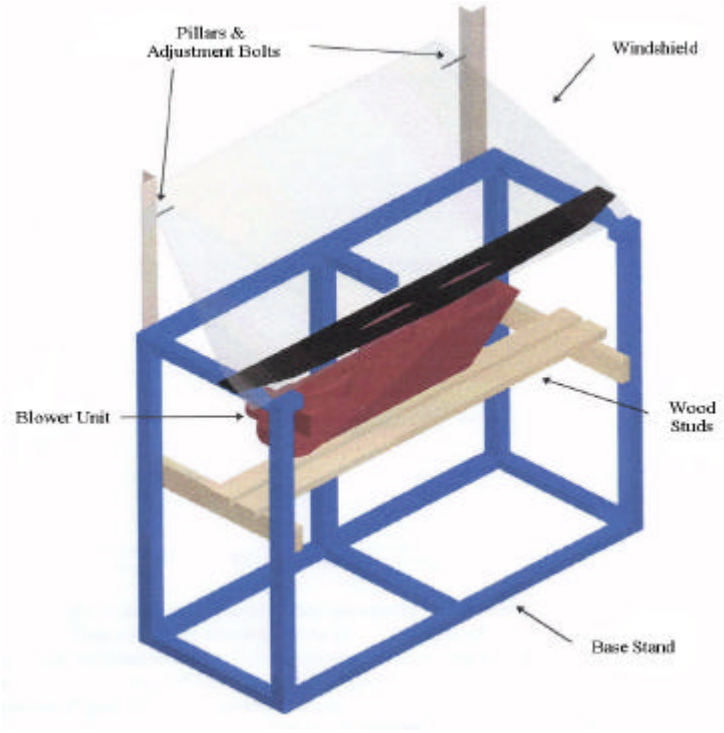

Figure 1. The experimental apparatus.

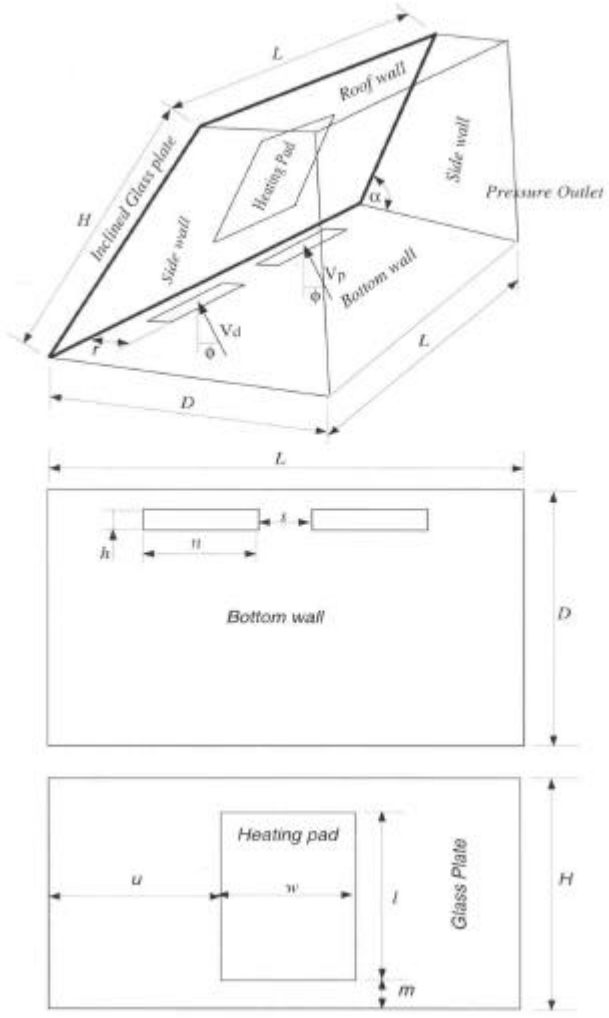

Figure 2. Schematic of the simulation domain.

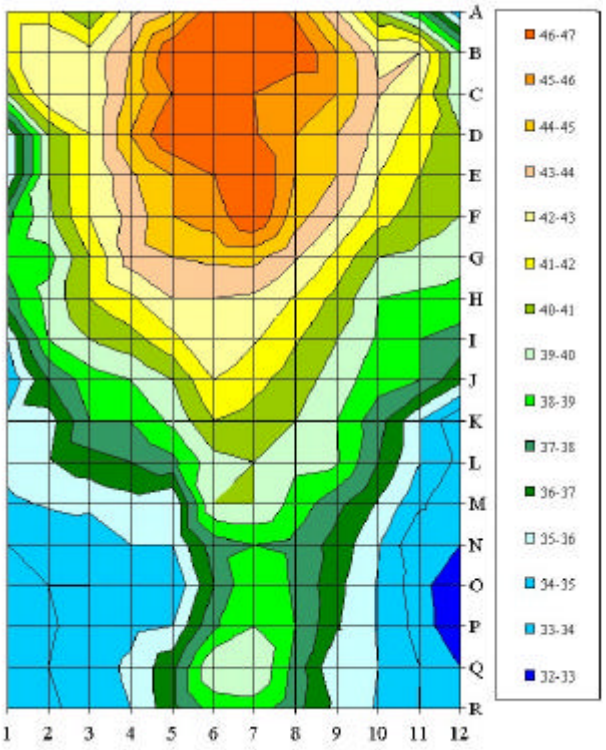

Figure 3. Experimentally based temperature contours on the heated area of the windshield.

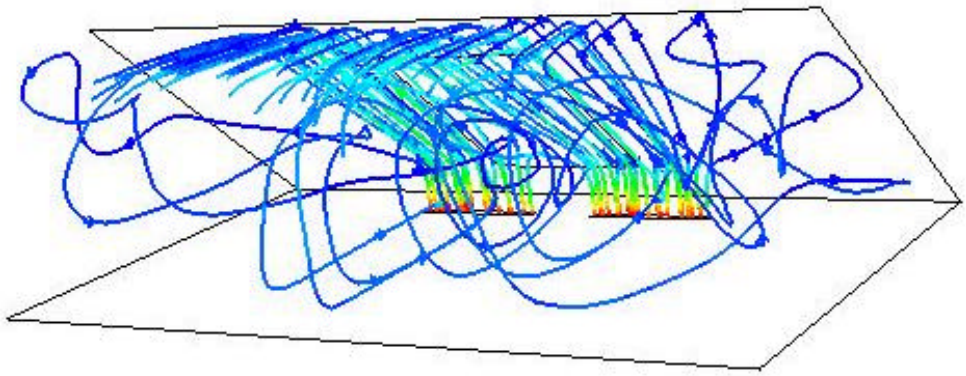

Figure 4. Particle tracks colored by speed show full three dimensionality of the flow field.

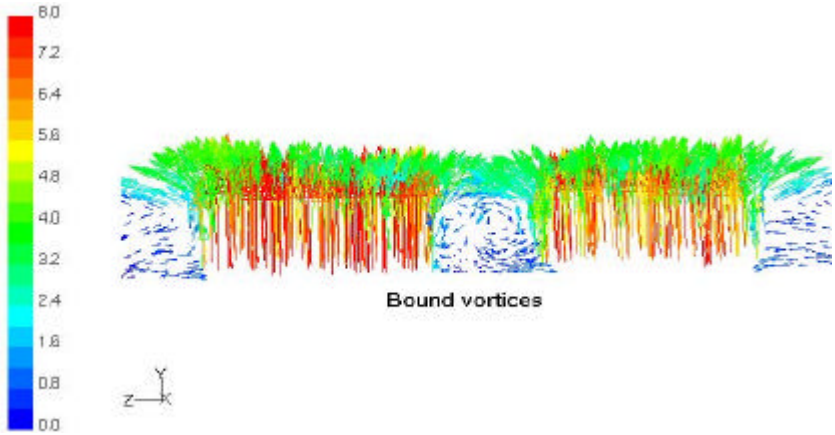

Figure 5. Velocity vector distribution on the plane cutting through the defrosters shows bound vortices.

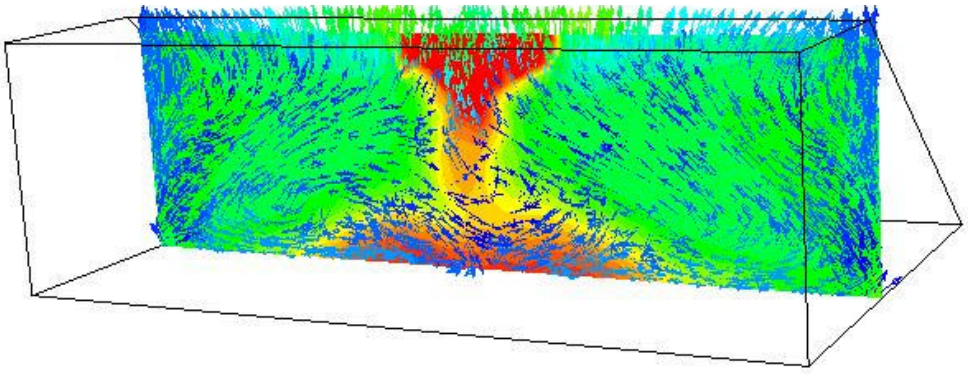

Figure 6. Velocity vector distribution on the vertical plane superimposed over the temperature distribution.

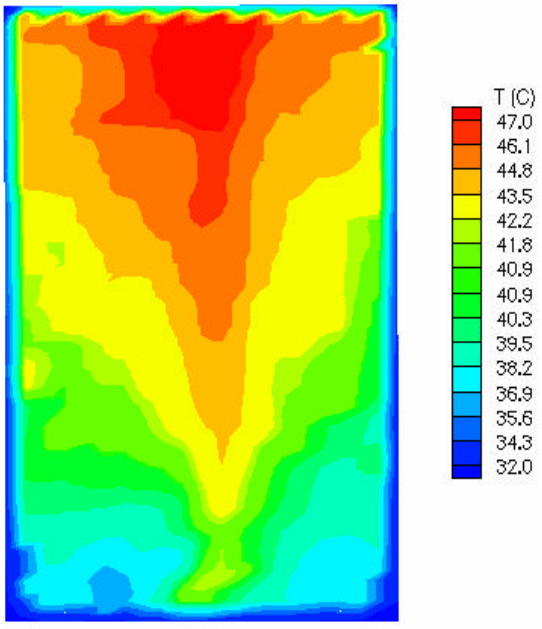

Figure 7. Temperature distribution on the inside surface of the windshield across the heating pad.

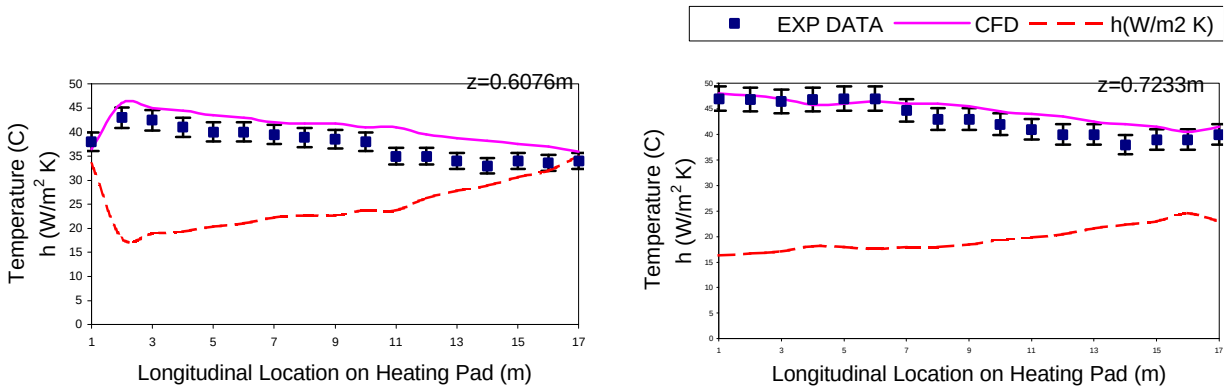

Figure 8. Validation of CFD results with experimental data at different locations on the heating pad.

Table 1. Calculated heat transfer coefficients (W/m^2 K) based on local temperature values

	A	B	C	D	E	F	G	H	I	J	K	L
A			25.4		19.9	17.1	17.1		21	25.4	29.4	43.3
B		21		19.9	17.1			17.1	18.9		21	27.3
C	25.4	21	22.3		17.9			18.9	18.9		22.3	27.3
D	38.7		22.3	18.9	17.1				19.9			
E	38.7	25.4	22.3		18.9		17.1	18.9	19.9	22.3		25.4
F			22.3		18.9		17.1		21			
G			23.7		19.9					25.4		
H			23.7		21	21				27.3		
I	38.7	27.3	25.4			21					29.4	
J	43.3			27.3	25.4	22.3					29.4	
K			29.4	29.4		23.7		25.4	27.3		38.7	49.1
L				32			25.4			32	38.7	
M					38.7	25.4	25.4					49.1
N			43.3	38.7	38.7		29.4				49.1	49.1
O	49.1	43.3	43.3		43.3		27.3					56.6
P					38.7		27.3	29.4				56.6
Q		43.3				25.4	25.4		38.7	38.7	43.3	
R	49.1			38.7								49.1

Table 2. Material properties used in the numerical simulation

	Air	Glass
Density (kg/m^3)	1.225	2500
Specific Heat (J/kg-K)	1006.43	750
Thermal Conductivity (W/m-K)	0.0242	1.4
Viscosity (kg/m-s)	1.7894e-5	